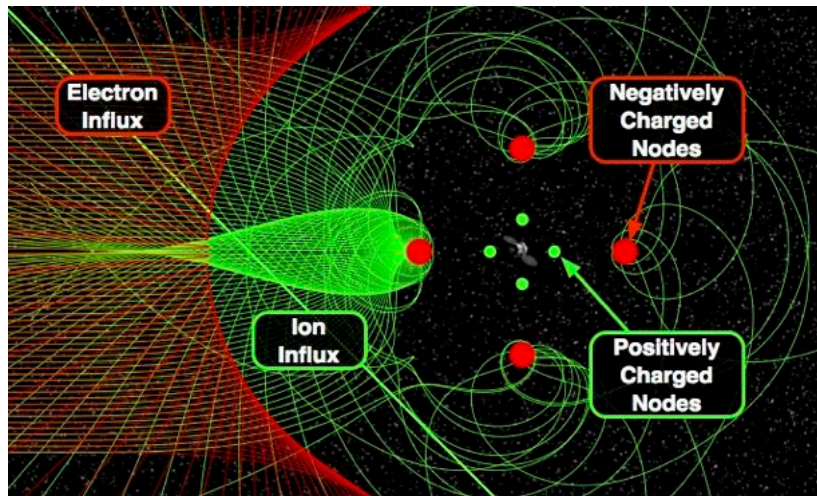


NASA Langley Supported Study (Contract # NNX11AJ80G)

Electrostatic Charge Deflection Experiments (Extended Study)

Final Report



Principal Investigator:

Hanspeter Schaub¹

University of Colorado, Boulder, CO 80309-0431

26 June 2012

¹ Associate Professor, hanspeter.schaub@colorado.edu, (303) 492-2767

Abstract

This report describes the research completed during a 6-month study at the University of Colorado on charge deflection using electrostatically inflated membrane structures (EIMS). The study is a follow-on to experiments performed in the summer of 2011 at the University of Colorado. The research is motivated by the desire to achieve active space radiation shielding using large lightweight gossamer space structures. The goal is to investigate if a charged Gossamer structure can perform charge deflections without significant structural instabilities occurring. In this study, experiments are performed with up to 10kV of membrane charging, and an electron flux source with up to 5keV of energy and 5mA of current. While these charge flux energy levels are much less than those encountered in space, the fundamental coupled interaction of charged Gossamer structures with the ambient charge flux can be experimentally investigated. Of interest are, will the EIMS remain inflated during the charge deflections, and are there visible charge flux interactions. Aluminum coated Mylar membrane prototype structures are created to test their inflation capability using electrostatic charging. To simulate the charge flux, a 5keV electron emitter is utilized. The remaining charge flux at the end of the test chamber is measured with a Faraday cup mounted on a movable boom. A range of experiments with this electron emitter and detector were performed within a 30x60cm vacuum chamber with vacuum environment capability of 10^{-7} Torr. Experiments are performed with the charge flux aimed at the EIMS in both charged and uncharged configurations. The amount of charge shielding behind and around the EIMS was studied for different combinations of membrane structure voltages and electron energies. Both passive and active shielding were observed, with active shielding capable of deflecting nearly all incoming electrons. The pattern of charge distribution around the structure was studied as well as the stability of the structures in the charge flow. The charge deflection experiments illustrate that the EIMS remain inflated during charge deflection, but will experience small amplitude oscillations. Investigations were performed to determine a potential cause of the vibrations. It is postulated these vibrations are due to the charge flux causing local membrane charge distribution changes. As the membrane structure inflation pressure is changed, the shape responds, and causes the observed sustained vibration. Having identified this phenomena is important when considering implying EIMS in a space environment. Additionally, this project included a study of membrane material impacts, specifically the impact of membrane thickness. Extremely thin materials presented new challenges with vacuum preparation techniques and rapid charging. The thinner and lighter membrane materials were successfully inflated using electrostatic forces in a vacuum chamber. However, care must be taken when varying the potentials of such lighter structures as the currents can cause local heating and melting of the very thin membranes. Lastly, a preliminary analysis is performed to study rough order of magnitude power requirements for using EIMS for radiation shielding. The EIMS power requirement becomes increasingly more challenging as the spacecraft voltage is increased, reaching MW to GW levels for larger MV voltages being considered to deflect cosmic radiation.

Table of Contents

| | | |
|----------|--|-----------|
| 1 | INTRODUCTION | 5 |
| 1.1 | Motivation | 5 |
| 1.2 | EIMS Background | 6 |
| 1.3 | Radiation Shielding Background..... | 8 |
| 1.4 | Project Scope | 9 |
| 1.5 | Research Team | 9 |
| 1.6 | Subject Inventions | 9 |
| 2 | EXPERIMENTAL SETUP | 10 |
| 2.1 | High Voltage EIMS Charging Setup..... | 10 |
| 2.2 | Charge Deflection Hardware Components..... | 11 |
| 3 | ELECTROMECHANICAL VIBRATIONS STUDY | 14 |
| 3.1 | Vibration Mechanics | 14 |
| 3.2 | Source of Vibrations | 15 |
| 3.3 | Electron Gun Trade Study..... | 16 |
| 4 | EXTENDED CHARGE DEFLECTION EXPERIMENTS..... | 18 |
| 5 | MEMBRANE MATERIALS STUDY..... | 22 |
| 5.1 | Materials | 22 |
| 5.2 | Experiments | 23 |
| 6 | SHAPE INVESTIGATIONS | 25 |
| 6.1 | Analytical Development for a Sphere | 25 |
| 6.2 | Electrostatic Simulations | 27 |
| 7 | POWER REQUIREMENT STUDY..... | 29 |
| 7.1 | Nominal Power Requirement | 29 |

| | | |
|------------|------------------------------------|-----------|
| 7.2 | SPE Power Requirement | 32 |
| 7.3 | GCR Power Requirement | 34 |
| 7.4 | Outlook..... | 35 |
| 8 | CONCLUSIONS | 37 |

1 Introduction

1.1 Motivation

Radiation shielding is an important design criterion for any space mission, especially those involving human space explorers. A long-term goal for NASA is to use lightweight structures for active radiation shielding to create safe habitation zones. An example of this is charged membrane structures deflecting the harmful radiation ion-flux as seen in Figure 1.1. This report describes an investigation into the use of electrostatic fields for radiation shielding through such charged membrane structures. The membrane structures consist of layers of conducting material which self-repel to inflate when an absolute charge is applied. The electrostatically inflated membrane structure (EIMS) is envisioned as a lightweight structure that can act as shield to charged particles.

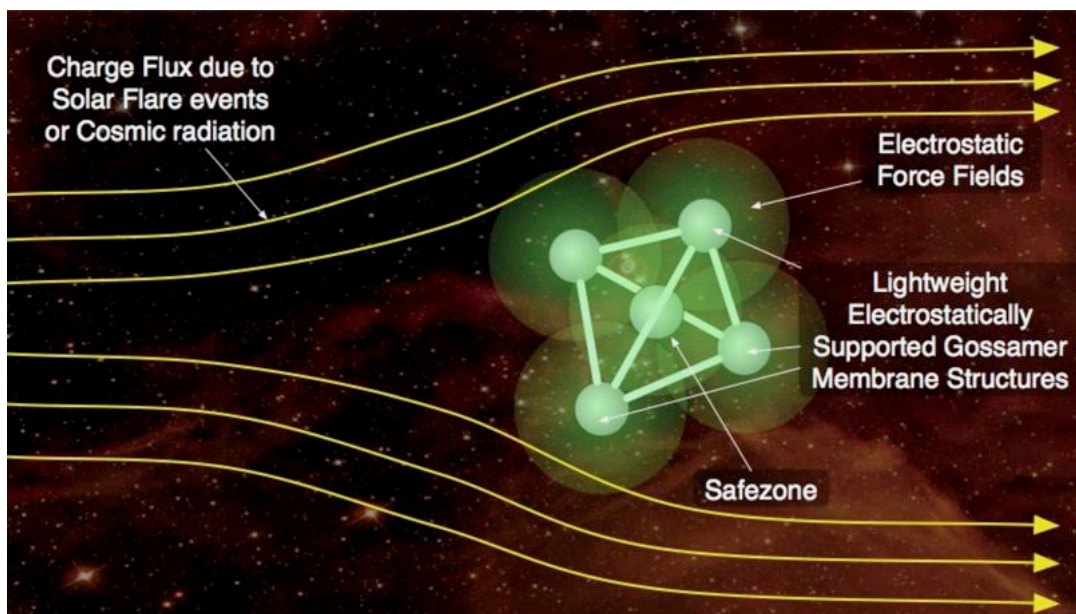


Figure 1.1: Concept illustration of radiation shielding with an electrostatically charged structure

An experimental setup was designed to study the use of EIMS for charge deflection. An electron source and detector were mounted on opposite sides of an EIMS in a vacuum chamber. Experiments were performed to study the radiation shielding capabilities, the charge deflection pattern, and the stability of the structure. The report will discuss the hardware and software development for experiments, the membrane structure shapes, as well as a discussion on power requirements.

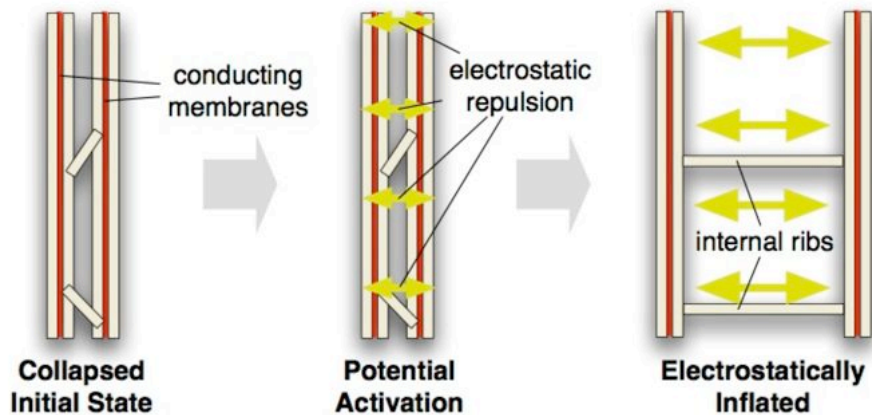


Figure 1.2: Illustration of electrostatic inflation of a membrane structure. The membrane interconnects (ribs) limit the amount of expansion and control the EIMS shape and thickness

1.2 EIMS Background

Electrostatically Inflated Membrane Structures or EIMS employ layers of lightweight membrane with a conductive coating along with active charge control to create inflationary electrostatic forces as shown in Figure 1.2. With this concept, extremely large deployed to stored volume ratios are feasible. The stored membrane structure will be packaged very tightly and does not require any pressurized gas storage devices. Rather, active charge control in the form of charge emission is employed to control the absolute EIMS potential. With EIMS it is feasible that the deployed structures are open shapes. Punctures due to micro-meteorites will have a negligible impact as this concept does not suffer from leakage concerns like gas-inflated Gossamer structures.

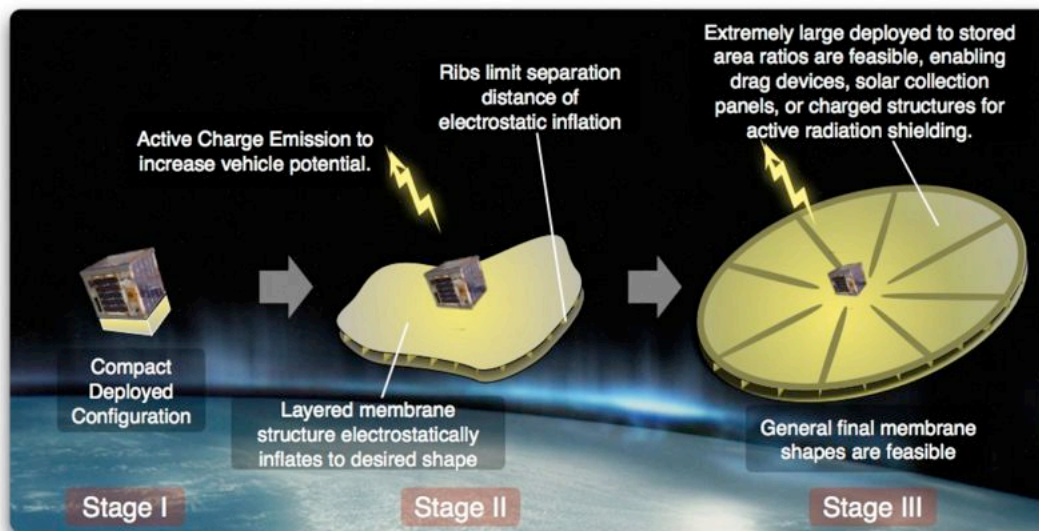


Figure 1.3: Electrostatic inflation concept illustration

An illustration of the EIMS concept deploying on a small satellite is shown in Figure 1.3. This concept of electrostatic inflation of membrane space structures is explored in earlier publications.^{2,3} The analysis in these references includes determination of the voltage required on a two-membrane sandwich structure to offset normal compressive orbital perturbations to the structure. The compressive pressures would tend to collapse the membrane structure, thus must be compensated by the inflation pressure. In GEO, solar radiation pressure is the dominant compression pressure of the orbital perturbations. In LEO, solar radiation pressure dominates until an orbit altitude of approximately 500km, under which atmospheric drag becomes the dominant pressure. To offset the normal compressive orbital pressures, it was found that hundreds of volts are required in GEO and a few kilovolts in LEO. Figure 1.4 illustrates a box-like membrane structure overcoming 1-g of gravity to inflated using a few kilovolts in atmospheric laboratory conditions.



Figure 1.4: Atmospheric Electrostatic Inflation Experiment of a Box-Like Membrane Structure

Many challenges to the electrostatic inflation concept exist, such as plasma Debye shielding, space weather, orbital perturbations which may tend to collapse the structure, and complex structural dynamics. In the space plasma environment, electrons and ions rearrange to maintain macroscopic neutrality when perturbed by an external electric field.⁴ This phenomena causes a steeper dropoff in the potential surrounding a charged object than would occur in a vacuum, thus limiting electrostatic force actuation, especially in cold, dense plasmas. In addition to Debye shielding, the plasma complicates charging of a spacecraft due to ram effects as a spacecraft moves through the plasma and also wake effects behind the moving craft. For the EIMS concept, it will be important to understand how the charge will flow around the structure and affect inflation. Experiments described within this report were aimed at studying shape stability during charge deflection experiments. Such tests require that the charging experiments are performed in a controlled vacuum chamber with high-quality pumps to avoid issues with ionization of a low-pressure atmosphere. For the experiments discussed in this report, the chamber achieved a vacuum of 10^{-7} Torr for inflation tests and 10^{-6} Torr for charge deflection experiments.

² Stiles, L. A., Schaub, H., Maute, K., and Moorer, D. F., "Electrostatic Inflation of Membrane Space Structures," AAS/AIAA Astrodynamics Specialist Conference, Toronto, Canada, Aug. 2–5 2010, AIAA- 2010-8134.

³ Stiles, L. A., Schaub, H., and Maute, K. K., "Voltage Requirements for Electrostatic Inflation of Gossamer Space," AIAA Gossamer Systems Forum, Denver, CO, April 4–7 2011.

⁴ Bittencourt, J. A., Fundamentals Of Plasma Physics, Springer-Verlag New York, Inc., 175 Fifth Avenue, New York, NY, 2004.

1.3 Radiation Shielding Background

Radiation shielding is a critical challenge with envisioned manned space exploration activities. The dangers of radiation to biological tissue must be well understood, and protection incorporated into any space travel concept. This is particularly true for long duration missions and travel beyond Low Earth Orbit. Radiation shielding can be accomplished with passive or active methods, or a combination of the two. Current designs employ passive damping where sufficient material is present to absorb enough of the harmful high-energy ion radiation. This concept has the benefit that no active control is required, and thus it provides a robust solution. One drawback of passive shielding is the mass of the materials required for adequate radiation safety. This mass is a challenge when designing interplanetary human explorations. A savings in the mass required to perform radiation shielding would enable significant mission cost reductions.

Use of electrostatic fields is one active method that provides an alternative to bulk material passive shielding.⁵ Other forms of active shielding include plasma shields, confined magnetic fields, and unconfined magnetic fields.⁶ Some of the challenges of active electrostatic shielding, such as high potentials and size limitations due to electrical breakdown, have deterred further research on the subject.⁷ In Reference 7, Tripathi challenges the claim that electrostatic shielding may be unsuitable and explores a feasible design for radiation shielding, as shown in Figure 1.5.

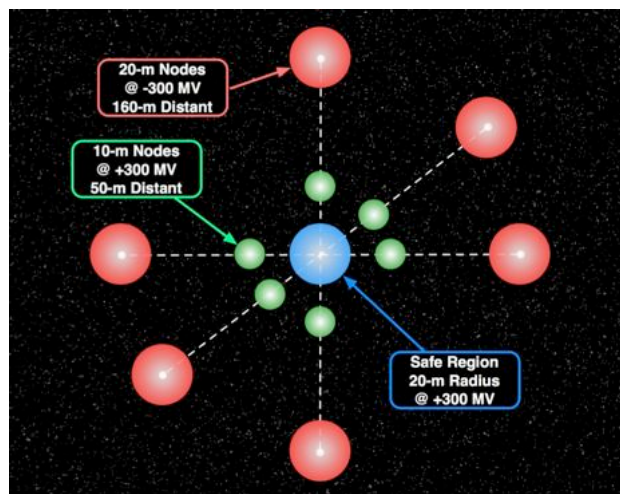


Figure 1.5: Electrostatic space radiation shielding concept

⁵ Spillantini, P., Casolino, M., Durante, M., Mueller-Mellin, R., Reitz, G., Rossi, L., Shurshakov, V., and Sorbi, M., "Shielding from cosmic radiation for interplanetary missions: Active and passive methods," *Radiation Measurements*, Vol. 42, No. 1, 2007, pp. 14 – 23, DOI: 10.1016/j.radmeas.2006.04.028.

⁶ Townsend, L., "Overview of active methods for shielding spacecraft from energetic space radiation," *Physica Medica*, Vol. 17, 2001, pp. 84–85.

⁷ Tripathi, R. K., Wilson, J. W., and Youngquist, R. C., "Electrostatic space radiation shielding," *Advances in Space Research*, Vol. 42, No. 6, 2008, pp. 1043–1049, DOI: 10.1016/j.asr.2007.09.015.

The 10-sphere design requires potentials of 300 MV, and would be used in conjunction with passive material shielding. The author notes that the ability to achieve 300 MV potential levels remains as future work. For EIMS applications, only potentials in the tens of kilovolts have been explored to study the ability to inflate and overcome membrane residual stresses, therefore investigating the feasibility of potentials beyond tens of kilovolts is part of future work. Radiation shielding capabilities of EIMS charged within a range of 0-5 kV are described in the results section of this report.

1.4 Project Scope

This report describes experiments performed as part of a 6-month study conducted at the University of Colorado at Boulder from December 2011 – May 2012. The CU facilities used for the study include a small vacuum chamber that is 30cm in diameter and 60cm long with pressures feasible to the 10^{-7} Torr range. Such a chamber was ideal for cost-effective initial deployment and shape testing of EIMS test concepts and charge bombardment experiments. This vacuum chamber, pumps, and high-voltage interfaces are owned by Dr. Zoltan Sternovsky of the University of Colorado. He is an international expert on dusty plasma physics and high-voltage charge transfer experiments. He provided guidance on the experimental setup, and his researchers helped Dr. Schaub's students learn how to use their facility. Without their help and knowledge on performing vacuum chamber charging experiments the 6-month project would not have been possible.

1.5 Research Team

The research for the study was led by Dr. Schaub's Ph.D. graduate student Laura Stiles, and supported by Paul Anderson and Carl Seubert. Laura led the hardware development and vacuum chamber test development and analysis. Project direction and advising were provided by Dr. Hanspeter Schaub with collaboration and support by Dr. Zoltan Sternovsky of the University of Colorado. One undergraduate student, Jack Mills, provided technical assistance with experiments. He aided in membrane structure construction, running experiments within the chamber, and developing macros to quickly analyze collected data.

1.6 Subject Inventions

No inventions were created as part of this research grant. The results have been published and reported in a conference paper and the N

2 Experimental Setup

The setup for the radiation experiments includes an electron gun at one end of a vacuum chamber and a Faraday cup positioned behind a membrane structure at the opposite end of the chamber. The electron gun will emit electrons and the Faraday cup will measure the current, allowing observation of the flow of electrons around an EIMS structure and providing insight into how an EIMS structure can be used for radiation shielding. The EIMS structure is charged with a high voltage power supply system external to the vacuum chamber. The concept is illustrated in Figure 2.1.

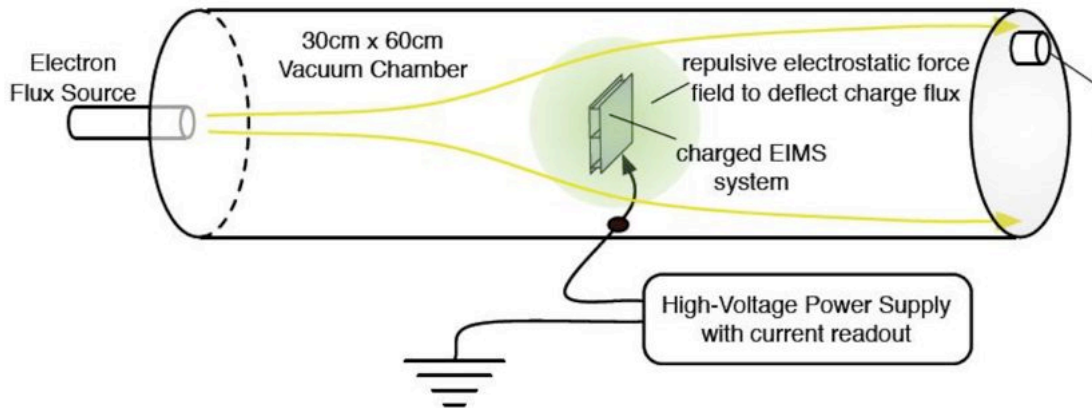


Figure 2.1. Concept illustration for the radiation shielding experimental setup

2.1 High Voltage EIMS Charging Setup

The first component of the experimental hardware that was designed and built was a high voltage EIMS charging setup. The charging setup is used to apply a desired voltage to the membrane structures for inflation.

Figure 2.2 displays a diagram of the setup. The high voltage is supplied by an Ultravolt 40A Series high voltage DC-DC converter. This device supplies up to -40kV to the membrane structures. The voltage magnitude is controlled by a user through a Graphical User Interface on a Macbook computer, as shown in Figure 2.3. A National Instruments USB-6008 data acquisition device is used to drive the power supply and also to record current and voltage data.

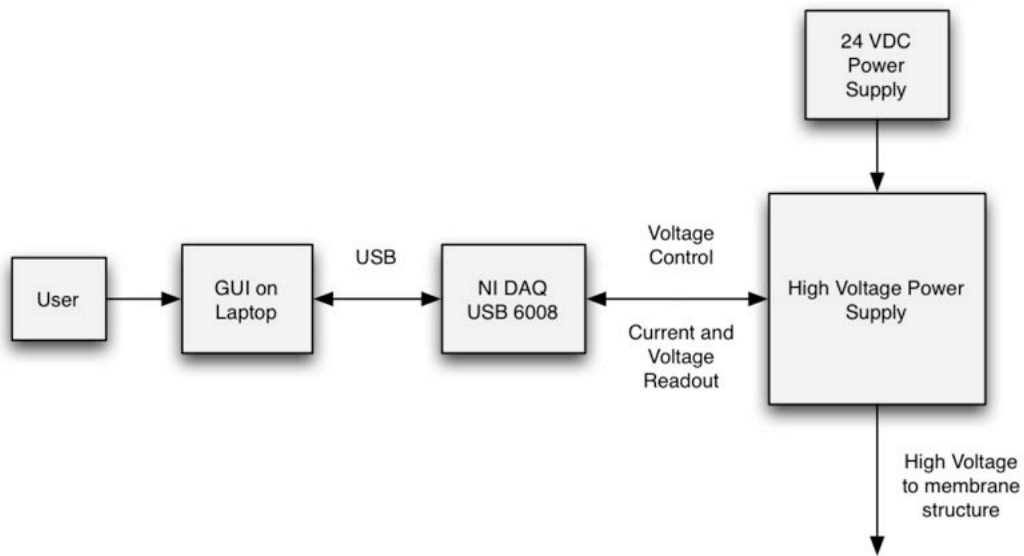


Figure 2.2. Block diagram of high voltage charging setup for membrane structures

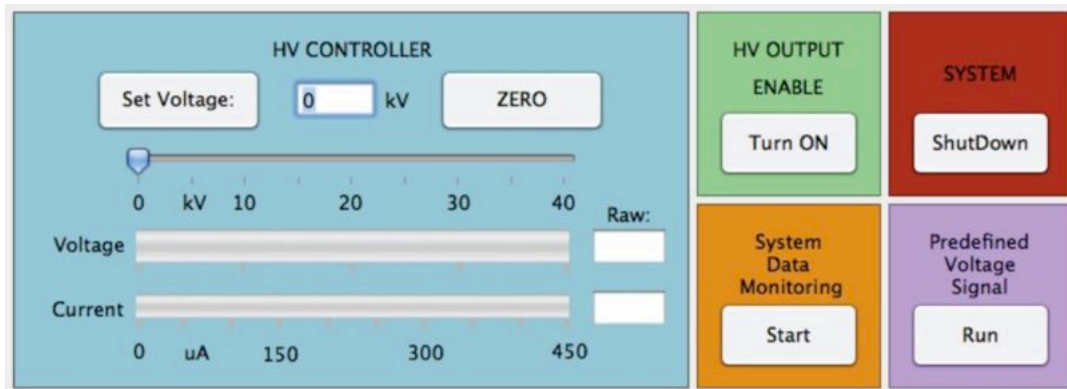


Figure 2.3. Graphical User Interface for operating the high voltage charging setup

This custom software allows the EIMS to be charged to a particular absolute voltage by either manually moving the voltage slider, or by running a predefined voltage history on the structure. For the following experiments that setup is such that the voltage is being held at a fixed value which charge flux and EIMS stability observations are made.

2.2 Charge Deflection Hardware Components

Figure 2.4 illustrates each of the components of the experimental setup. A summary of the setup is as follows: the electron gun is heated and electrons produced by thermionic emission are accelerated from the filament, biased to -5 kV, toward the grid, which is

grounded. A membrane structure hangs between the electron gun and a detector to read the current behind and around the structure.

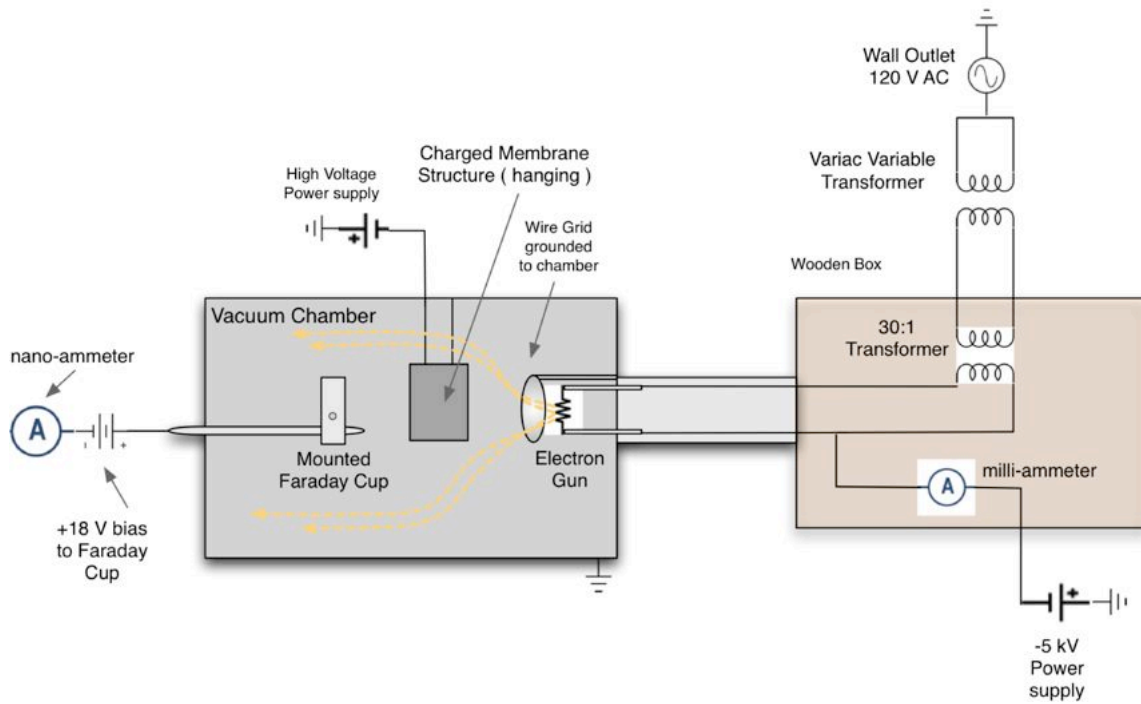


Figure 2.4. Radiation Experiment Hardware Diagram

Figure 2.5 shows the constructed electron emitter. The filament is heated and electrons accelerated off by the electrostatic field between the filament and the grounded wire mesh.

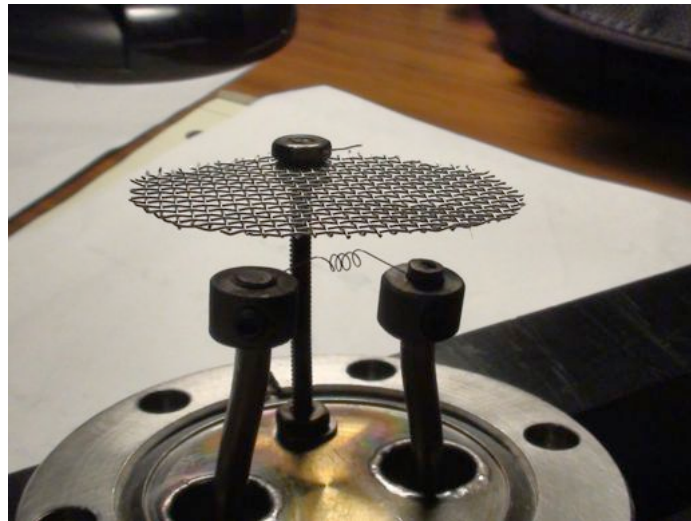


Figure 2.5. Electron gun filament and wire mesh

The filament is constructed of 5mil coiled Tungsten wire. The length of the Tungsten wire was chosen based on the resistivity of the metal, ρ , and the electrical resistance, R . The

resistivity of Tungsten near the melting point is approximately 10^{-6} Ohm-meters and the electrical resistance was measured in the lab to be 2-3 Ohms. Using the below equation, the 5 mil wire (cross sectional area, $A=1.3e-8$) could have a length, l , of approximately 3.8 cm.

$$l = R \frac{A}{\rho}$$

The current emitted from the tungsten coil can be tuned by changing the setting of the Variac variable transformer. The higher the AC current supplied to the coil, the higher the temperature, thus more electrons can be accelerated toward the grid. The high voltage power supply providing the DC bias to the coil is current-limited at 5 mA, therefore the maximum emission current is 5 mA.

The FC-70 Faraday cup was chosen as the device to detect current inside the chamber. The detector has a small aperture into which electrons can flow to measure the ambient current. The FC-70, shown in Figure 2.6 is mounted onto an aluminum plate with a collar attached with vacuum epoxy. The collar allows for mounting the device onto a rotatable vacuum feedthrough probe. The rotatable probe allows the Faraday cup to sweep through an angular range of approximately 120° thus providing positioning both behind and to each side of the membrane structure.



Figure 2.6. Mounted Faraday cup with collar for attachment to vacuum feedthrough

The output of the Faraday cup is connected to a digital multimeter with DC current resolution to picoAmps. A battery is located in the path between the nano-ammeter and the Faraday cup. The battery is a combination of the two 9 Volt batteries connected in series to bias the Faraday cup by 18 V. This small voltage helps to eliminate low-energy secondary electrons from entering the aperture of the Faraday cup.

3 Electromechanical Vibrations Study

A key research focus of the charge shielding experiments was to explore the cause of small structural vibrations observed during charge bombardment of EIMS. This section describes the nature of the vibrations as well as the experiments to investigate to the cause.

3.1 Vibration Mechanics

The experiments show that the membrane structure is stable, in the sense that it does not collapse or undergo major shape changes, in all of the ranges of particle flows created (up to 5mA emission current and energies up to 5keV). However, small structural vibrations were discovered when the structure is charged and the electron gun is emitting a flow of electrons. To observe the vibrations, the membrane structure must be electrostatically inflated while the electron gun is emitting electrons. No vibrations are present with an uncharged membrane structure in the electron flux.

The vibrations are seen at both very low currents and the currents near the maximum of 5mA. The vibrations, however, are not seen through the full continuous sweep of currents. Rather, at particular charge flux and electrostatically inflationary pressure combinations a resonance-like vibration appears. If the EIMS voltage is changed upwards or downwards, the vibrations can cease until new critical conditions are achieved. Similar patterns are seen for the full range of membrane structure voltages (0 to 10 kV) and electron energies (0 to 5 keV).

Figure 3.1 is shown to convey the magnitude of vibrations in the structure. It is difficult to capture the small oscillations, but a difference can be seen in the membrane shadows of Figure 3.1. The vibrations are of small magnitude and ripple across the membrane structure.

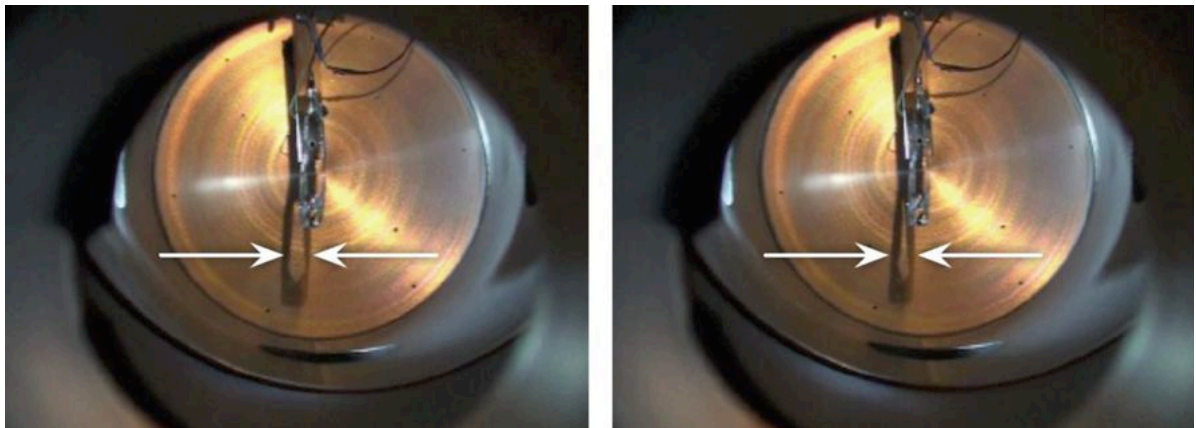


Figure 3.1: Photos of vibrating membrane structure. Vibration amplitude illustrated through shadow

A Strobotac stroboscope was used to investigate the frequency of the vibrations. Often, there were several different vibration frequencies present at a given instant. This indicates a complex ripple of vibrations is present as small shape changes occur, not just a single standing vibration. The primary frequencies measured were around the 4 Hz range. The vibrations experiments were also performed with different membrane

structures. One of these structures was constructed from two solid 8 x 10 cm sheets with additional weight at the bottom to tension the structure, as seen in Figure 3.2.

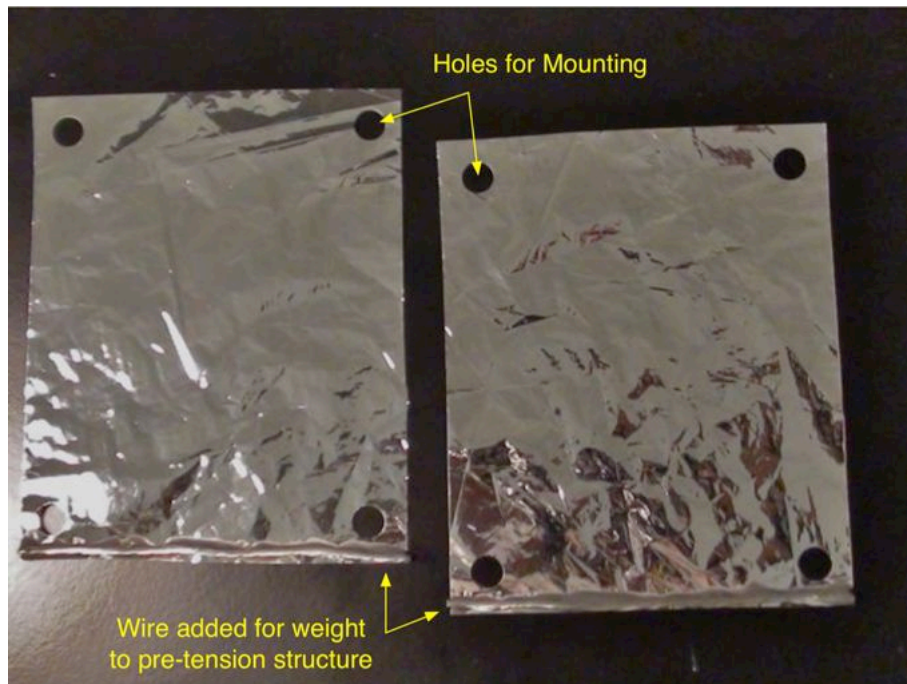


Figure 3.2: Weighted structure for vibrations experiments

The stroboscope was used to determine the approximate frequency of vibrations in the pre-tensioned structure. The vibrations were found to be near 8 Hz, approximately twice the frequency of the previous unweighted structures. The vibrations were also more consistent through the entire membrane.

3.2 Source of Vibrations

Several potential sources of such vibrations were investigated and eliminated. First, it is possible that the deflected charge flux imparts a sufficiently large momentum exchange with EIMS to cause this rippling. To investigate this possible cause, experiments with a single membrane sheet were performed. None of the single-sheet experiments, charged or not charged, showed any visible vibrations, even sweeping through all feasible electron energies and all electron currents. These results suggest that the vibrations are un-likely caused by a transfer of momentum. Otherwise, vibrations or deflections would have been seen with single sheet experiments.

Secondly, the electron flux itself could be a source of these vibrations if the electron gun emitted flux is not steady, but has frequencies near 4Hz. To investigate this possible vibration cause, the electron flow output signal from the emitting gun is studied with an oscilloscope. The Fourier transform function of the oscilloscope is used to determine frequencies present in the driving current signal. The only significant frequencies present were the power line frequency of 60 Hz and a very high frequency in the kiloHertz range. Neither of these frequencies are in the 4Hz range of the observed structure vibrations.

Thirdly, fluctuations in the EIMS external power supply performance could cause EIMS vibrations. In essence, if the actual EIMS voltage is not held steady, but cycles in the presence of the external charge flux, then these voltage variations would directly result in the electrostatic inflation pressure varying. As a result, the EIMS structure would slightly deflate and inflate. An oscilloscope is used to examine the output of the power supply which charges the membrane structure. The power supply has an internal feedback loop to ensure a digitally commanded reference voltage level is maintained. The measure output signal provides a measurement of how well this voltage is being held constant. It was speculated that the power supply may be overcompensating as the external charges from the electron gun change the charge on the structure. It was found, however, that the power supply output frequencies, with and without the EIMS vibrations present, showed no significant difference. In fact, the power supply fluctuations were very small, barely observable, and more than an order of magnitude larger than the observed EIMS vibrations. Thus, it is concluded that the power supply did not provide first order contributions to the EIMS vibrations. Otherwise, output power variations during EIMS vibrations would leave a unique fingerprint.

Finally, the question remains, what is driving these EIMS vibrations under particular electron flux and electrostatic inflation pressure conditions. The hypothesis is that the membrane surface vibration is a result of local surface charge density variations caused by the charge flux. As the charge density, σ , varies, then the local electrostatic inflation also changes. Since the EIMS system is in equilibrium between the 1-g gravitational forces attempting to compress the structure, and the electrostatic pressure inflating the structure, a small change in electrostatic pressure will negate this equilibrium and result in a local shape deformation, outward or inward. This shape change, in return, will cause a change in the surface normal electrostatic field which impacts the near-surface charge flux.

Analytical or numerical proof of this hypothesis will require considerable effort to model the time-varying flux and structural response. However, thus far, all experimental results support a dynamic coupling between the charge flux and the local charge distribution, resulting in the observed small magnitude vibrations. Further, note that this hypothesis requires the structure shape to be in equilibrium between competing electrostatic pressure and compressing gravity forces. This raises the question if such EIMS vibrations would manifest if the structure were in space without any acceleration present. If the electrostatic pressures are sufficiently large, here the shape inflation is not limited by gravity, but by internal support structure and membrane surface tension. Thus, a loss in pressure will not result in a shape change until the pressure is less than an externally compressing perturbation. In the absence of gravity, a gravity-like perturbation must still be considered if the structure is accelerated through an orbital maneuver. In particular, orbital maneuvers with EIMS are most likely to be performed with fuel-efficient low-thrust technologies. Thus, the future work investigating modeling and predicting such vibration behavior is of great importance.

3.3 Electron Gun Trade Study

A study was performed to evaluate a new design for the electron gun. The current design consists of a tungsten filament and a biased wire mesh to accelerate electrons. One consideration was to purchase a commercial electron gun. Commercial electron guns provide a wide array of options, including various electron energies, emission

currents, beam angles, and pulsing capabilities. Several of the low and medium energy options investigated from Kimball Physics would be appropriate devices, yet the price range was beyond the budget of the current research project. Electron gun prices were shared with the sponsor. Commercial options will remain as a possibility in the future for a more controlled, focused electron beam.

Besides commercial options, modifications to the current electron gun were considered. In particular, deflection plates for the electron gun would aid in focusing the beam of electrons. This idea is similar to a cathode ray tube, as seen in Figure 3.3⁸, where deflection plates are used to control the direction of the stream of electrons with an electrostatic field.

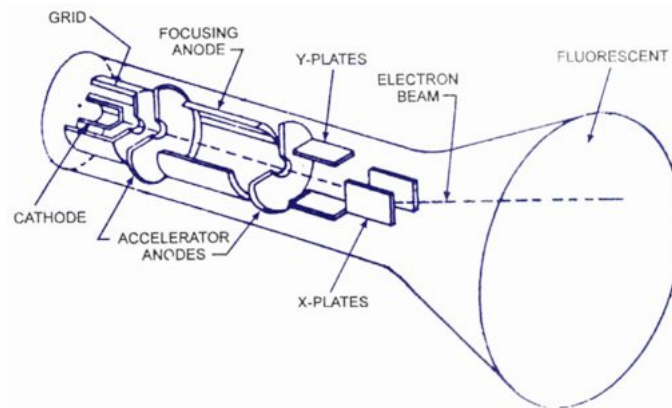


Figure 3.3: Cathode Ray Tube schematic showing deflection plates used to control the path of electrons

Another similar option is a biased ring or disc through which the electrons would pass to refine the spray of the electron gun into a more directed stream. Due to the geometry of the current electron gun, any modification would involve a complete rebuild of the device. However, at this stage of the research such enhancements were found not to be necessary. As will be seen in the later section, the University of Colorado was able to obtain good three-dimensional charge wake measurements about EIMS in the test chamber. Future work with a more focused charge emission will allow for edge and slot charge wake effects to be experimentally studied that were beyond the scope of this small study.

⁸ <http://www.circuitstoday.com/crt-cathode-ray-tube>

4 Extended Charge Deflection Experiments

Experiments with a charged structure in the electron stream were performed to understand the charge flow patterns around the electrostatically inflated membranes and also to study the charge deflection capability of low energy electrons. A Faraday cup position is rotated within the chamber to obtain a sweep of charge flux measurements down-stream of the EIMS. The probe on which the detector is mounted allows for rotation through approximately 120 degrees. Further, the probe can be positioned at different distances behind the EIMS. This allows for a three-dimensional measurement to be taken to study the mean charge wake behavior down-stream of the EIMS. Measurements of detected current are recorded as the probe and detector are swept through the physically feasible angular range. The rotation of the detector is illustrated in Figure 4.1. 3D surface plots are used here to represent the data from these experiments.

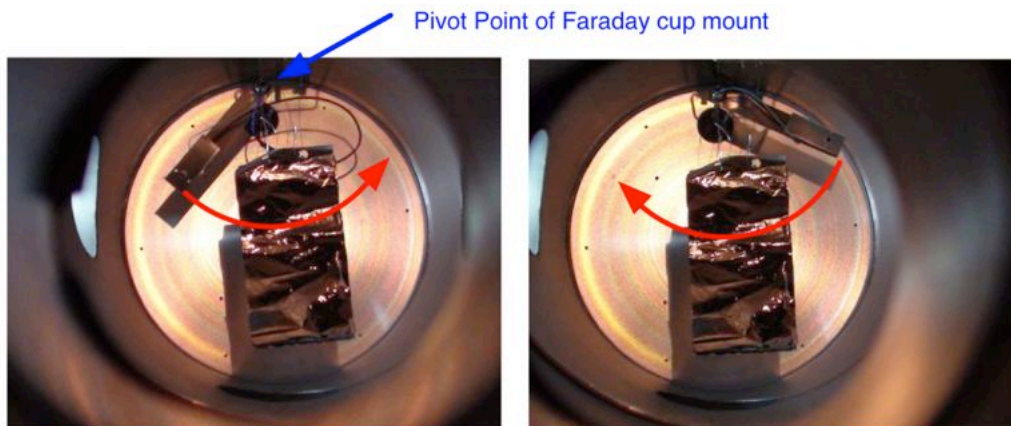


Figure 4.1: Rotation of the Faraday cup around the membrane structure

The first experiments were performed without a membrane structure in the vacuum chamber. The setup without a membrane structure allowed for determining a baseline of the natural charge flow patterns within the chamber. A 3D surface plot with the data collected with no structure is shown in Figure 4.2. The charge drop-off with increased distance from the electron gun is seen, as well as a variation as the detector is rotated from one side of the chamber to the other side.

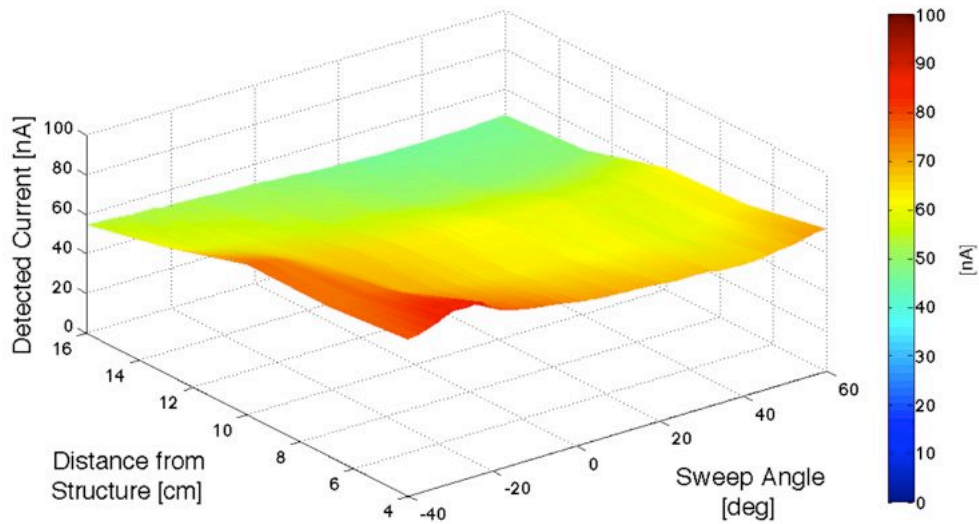


Figure 4.2: Electron flux with no membrane structure present (baseline flux)

Next, in Figure 4.3 the uncharged EIMS is added to the chamber, and subjected to a similar charge flux. The multi-micron thick aluminum coated Mylar is too thick for the 5keV electrons to penetrate. Thus, this result illustrates how much of the charge flux blocking is simply due to an uncharged EIMS. The electron flux directly behind the structure (approximately -20 to +15 degrees) drops from the 70 nA range down to the 25 nA range.

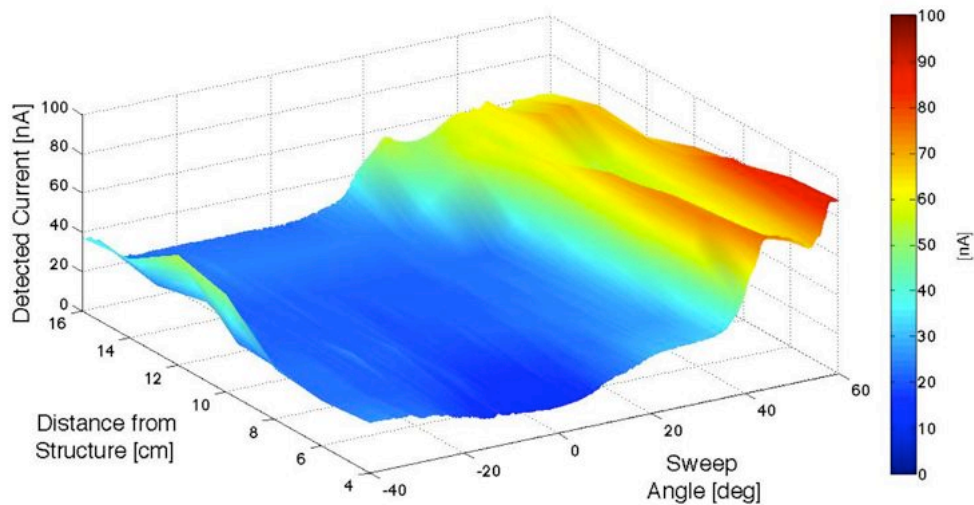


Figure 4.3: Electron Flux behind charged and uncharged EIMS of size 8 x 10cm

Next, the same data collection was performed with a charged structure at 4kV and 8kV. These two voltages were chosen such that one voltage was below the energy of the electron gun (5 keV) and one above. The surface plots are shown in Figure 4.4 for the 4 kV charging level and in Figure 4.5 for 8kV charging level.

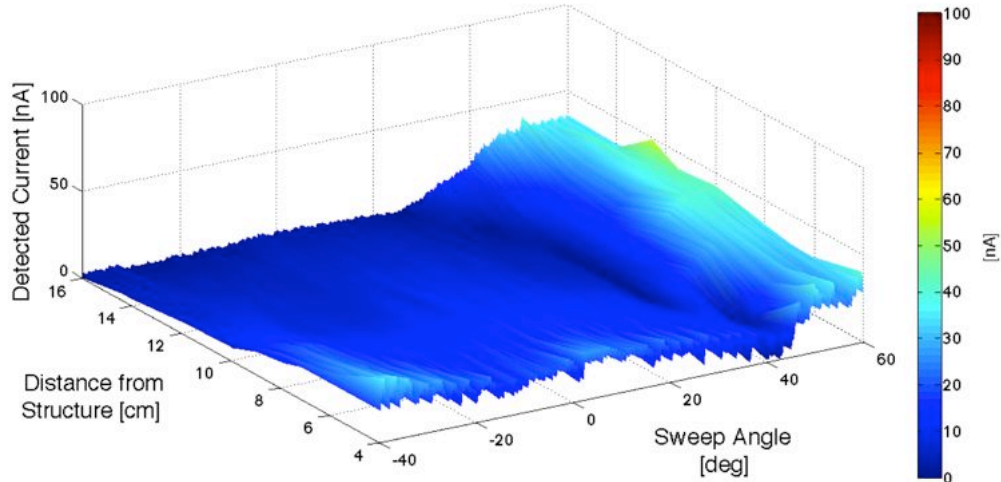


Figure 4.4: Electron Flux behind charged and EIMS of size 8 x 10cm charged to 4 kV (below electron energy)

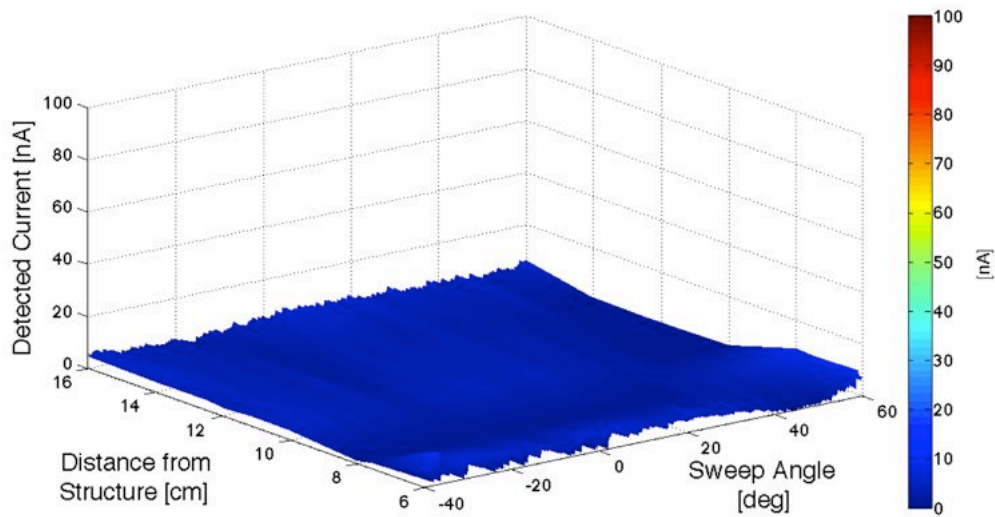


Figure 4.5: Electron Flux behind charged and EIMS of size 8 x 10cm charged to 8 kV (below electron energy)

When the structure is at 4kV and below the electron energy, there is still current in the 20 nA range behind the structure. There is an overall drop, however, in the amount of current detected anywhere behind or to the side of the structure. When the structure is charged to 8kV, there is another big drop in the current levels detected. All recorded

currents are below 12 nA and are in the single digit nA range behind the structure. These plots clearly show the low-energy electron shielding capabilities of a charged membrane structure.

5 Membrane Materials Study

A brief study of membrane materials was performed as a part of this project. In experiments prior to this project, EIMS had utilized only one membrane material: $\frac{3}{4}$ mil aluminized Mylar. Here, thinner materials are considered to observe and compare inflation capabilities and vibration mechanics.

5.1 Materials

Samples of two new materials were obtained for this project: $\frac{1}{4}$ mil Aluminized Mylar and $\frac{1}{3}$ mil Aluminized Kapton. These thinner materials have presented challenges in preparation for the vacuum chamber. The Aluminized Kapton material begins to warp after a prolonged period in the ethanol sonic bath, thus required development of new cleaning procedures. A photo of the warped membrane is shown in Figure 5.1.



Figure 5.1: Warped membrane following ethanol sonic bath

Another membrane issue that was encountered with the thinner materials is melting at the point of contact with the charging wire. This was observed with the $\frac{1}{4}$ mil Aluminized Mylar and is shown in Figure 5.2. This is likely due to the high current when rapidly charging the membrane structures. This melting was never encountered with the $\frac{3}{4}$ mil Aluminized Mylar. When using these thinner materials in the future, slower charging may be required to avoid high currents that may melt the material. This important result illustrates that charging currents must be considered when designing electrostatic charge deflection surface. While the membranes provide a novel light-weight solution, their thin conducting coating can provide increased electrical resistance when attempting to impart charge with a power supply. If the current is too large, i.e. the voltage change is rapid as experimentally performed with these thin membrane materials, the heating is sufficient to plastically deform and damage the membranes. Thus, while electrostatic inflation with the lighter membrane materials were possible, additional thermal considerations must be considered.



Figure 5.2. Melted membrane from contact with charging wire

5.2 Experiments

Inflation tests were performed in a vacuum environment with the $\frac{1}{4}$ mil Aluminized Mylar. Figure 5.3 shows the new structure inflated to 8 kV in the vacuum chamber.



Figure 5.3: The $\frac{1}{4}$ mil membrane structure inflated in the vacuum chamber

The thin structure inflated with slightly lower voltages than those required for full inflation of the thicker, $\frac{3}{4}$ mil material structure. Other factors, however, such as vacuum preparation techniques, were required to change for the thinner material structure. The

cause for less required voltage, therefore, cannot definitively be attributed to the thinner material. However, at this stage of the research the increased inflation capability is in line with the expected behavior of having a lighter, more flexible membrane.

6 Shape Investigations

Two studies were performed related to the membrane structure shape. First, an analytical development is presented which describes voltage requirements for an electrostatically inflated sphere and also tolerable accelerations of the sphere. Second, numerical electrostatic simulations are presented which were performed to understand the mechanics behind inflation of the membrane structures used in experiments.

6.1 Analytical Development for a Sphere

A study was performed to understand the voltage requirements for an electrostatically inflated sphere to offset orbital perturbation that may tend to collapse the structure. The mathematical development is as follows.

The electrostatic potential energy of the charges on the sphere is described by:

$$U = \frac{1}{2} \int V \sigma dS = \frac{1}{2} VQ$$

As the spacecraft potential is the parameter that is controlled, this can be rewritten as:

$$U = \frac{1}{2} CV^2 = 2\pi\epsilon_0 V^2 R$$

To find the force, we use the derivative of the potential energy:

$$F = \frac{dU}{dR} = 2\pi\epsilon_0 V^2$$

This is the total force acting on the sphere, but we are interested in pressure. The surface pressure would be:

$$P = \frac{F}{A} = \frac{F}{4\pi R^2} = \frac{\epsilon_0 V^2}{2R^2}$$

Figure 6.1 shows the relationship between voltage on the sphere and the pressure on the surface for sphere with a 1-meter diameter.

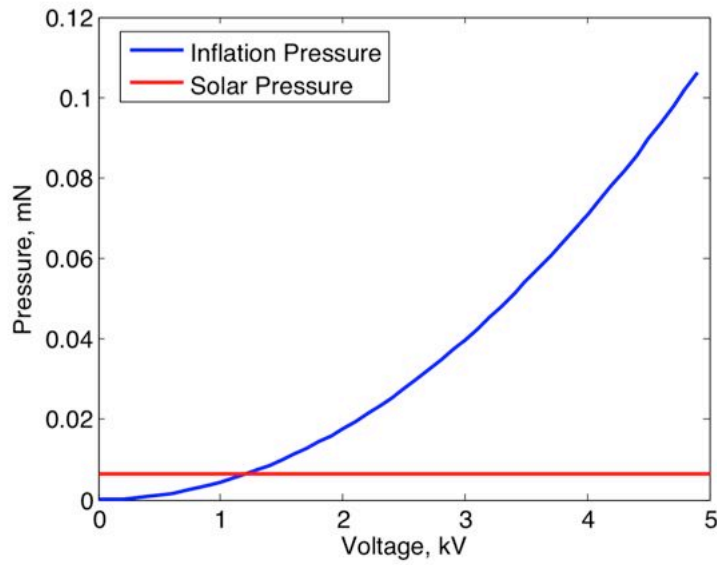


Figure 6.1: Electrostatic pressure and voltage relationship

For GEO, solar radiation pressure is the largest orbital perturbation. This has a constant value of approximately $6.4 \mu\text{N}/\text{m}^2$ and is shown as a line on Figure 6.1. As seen on the plot, the required sphere voltage to offset this compressive solar pressure is approximately 1.2 kV.

Examining the required pressure to offset solar radiation pressure across a range of sphere radii, it is seen that the required voltage remains feasible up to large craft sizes of 30 m radii. This is shown in Figure 6.2.

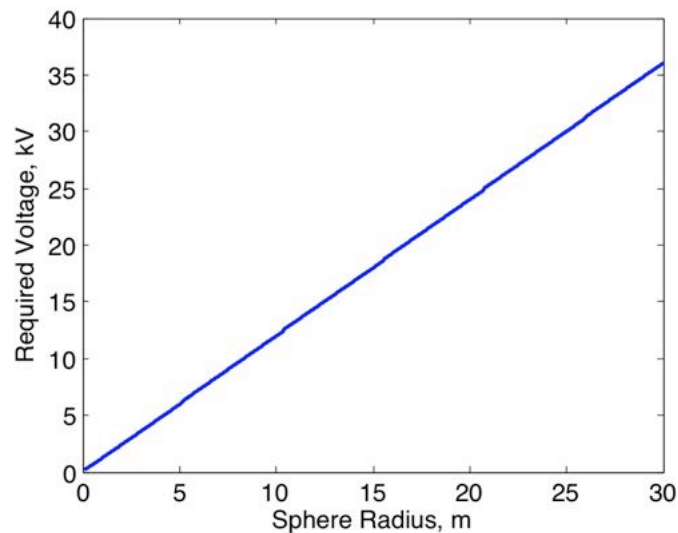


Figure 6.2: Voltage to offset solar radiation pressure for a range of sphere sizes

Similarly, a study was performed to understand the level of acceleration that an inflated sphere can withstand before beginning to collapse. Using a simple spring mass model of

the inflated structure, a range of sphere radii and sphere voltages were studied. The results are shown in Figure 6.3. Higher voltages allow greater accelerations whereas larger radii limit the acceleration.

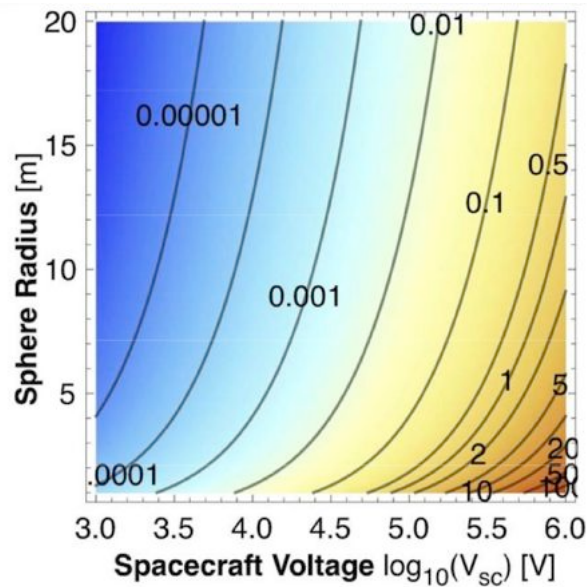


Figure 6.3: Allowable G-forces for an inflatable sphere

6.2 Electrostatic Simulations

To numerically study the electrostatic characteristics of different membrane shapes, the 3D electrostatic solver software 'Maxwell 3D' was utilized. Maxwell 3D allows simulation of the electrostatic forces and fields, capacitance, and charge distributions of user-defined geometries. The study performed was to investigate the electrostatic benefits of the membrane material cut-outs in the structures which inflate well in the laboratory and vacuum environment. Figure 6.4 shows the geometry of the cut-out structures and Figure 6.5 shows a solid membrane, each showing the electrostatic charge distribution given the same applied voltage. Notice in Figure 6.5 the increased charge distribution in the region of the membrane cut-outs. The magnitude of the charge distribution at these edges is nearly a 40% improvement of the charge distribution in the same location of the solid membrane. This increased charge yields a larger electrostatic force and therefore, a greater inflation pressure. Further, a non-solid membrane concept will enable further mass savings.

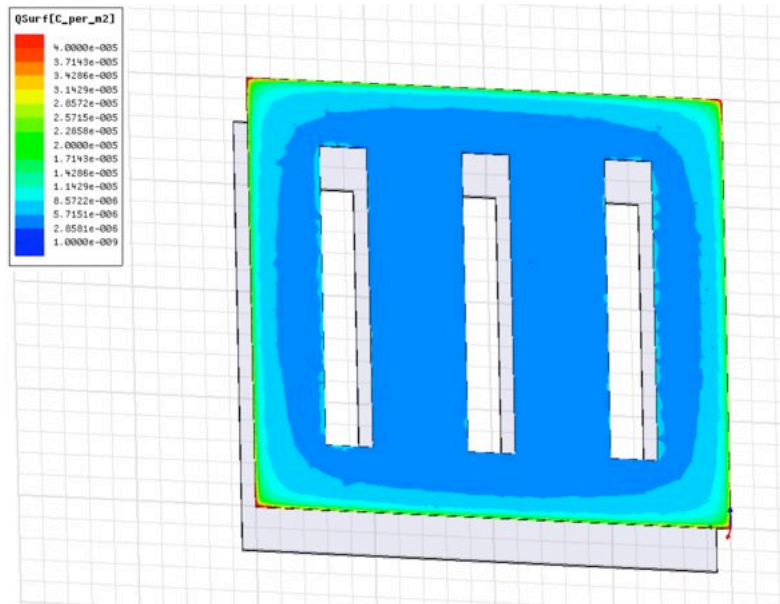


Figure 6.4: Charge distribution from electrostatic simulation of cut-out membrane structure

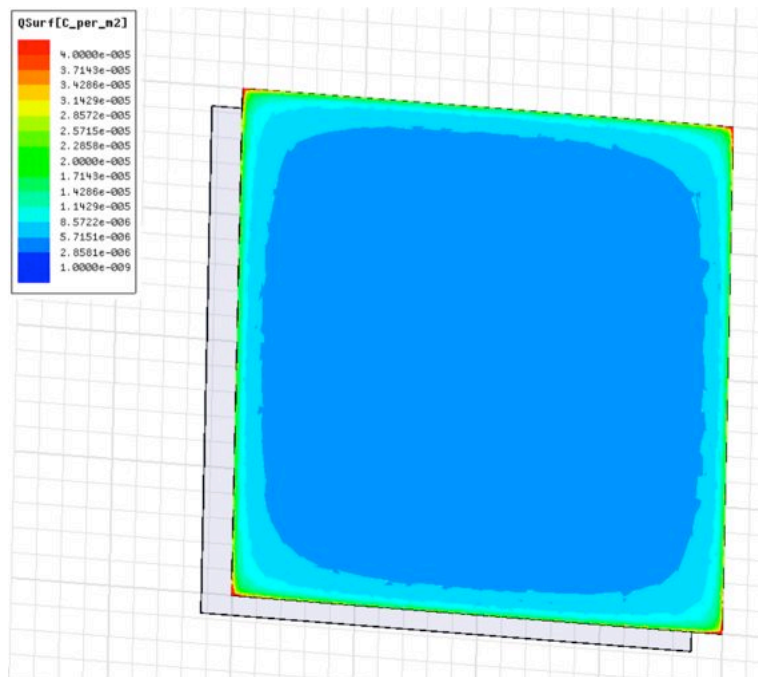


Figure 6.5. Charge distribution from electrostatic simulation of solid membrane structure

7 Power Requirement Study

The question of power requirement is a serious consideration for active space radiation shielding systems, including the electrostatic deflection scheme considered in this study. Thus, to supplement the electrostatic charge deflection experiments, a simplified analytical power assessment was performed to provide an approximation as to the order of magnitude of power required to maintain fixed voltage in a variety of representative plasma conditions. To obtain preliminary estimates of expected power levels, the power required to maintain a single sphere in a space plasma environment with a photo-electron current is considered. The charged spheres will create complex charge wake behaviors which impact the individual power needs of a multi-sphere setup. Such level of detail is well beyond the current scope of this project. Rather, the single-sphere power study illustrates if the low-energy, nominal space environment dominates the power evaluation, or if the high energy solar and galactic particles must be considered as well.

Section 7.1 provides an assessment of the nominal power requirement for maintaining a fixed electrostatic potential within the ambient deep space plasma environment. Sections 7.2 and 7.3 quantify the power impact incurred by typical solar particle events (SPE) and galactic cosmic radiation (GCR), and Section 7.4 offers an outlook as to the challenge of developing an electrostatic radiation shielding scheme that is robust *and* power-efficient.

7.1 Nominal Power Requirement

Preliminary power computations were performed to evaluate the practicality of maintaining a fixed potential within plasma conditions representative of deep space. Currents incurred by local ion and electron densities and the photoelectric effect are incorporated in these analytical power estimates; secondary emissions and backscattered electrons are neglected. For an isolated EIMS node with a 10-meter radius and active charge control device, the net plasma current flow is approximated as:

$$I_{net} = I_e - I_i - I_{pe} \pm I_{cc}$$

where I_e and I_i denote currents generated by the ambient electron and ion populations, respectively, I_{pe} is the current due to photoelectric scattering, and I_{cc} is the charge control current. To maintain a fixed spherical EIMS potential, the charge control device is employed to drive $I_{net} = 0$, such that I_{cc} is given by:

$$I_{cc} = I_e - I_i - I_{pe}$$

Assuming that the ambient plasma is comprised of electron and proton populations modeled with single-Maxwellian distributions, total electron and proton currents are developed for positively and negatively-charged EIMS with Mott-Smith and Langmuir attraction and Boltzmann repulsion:⁹

$$(I_e - I_i)|_{V_{sc} < 0} = J_{0e}A_n \exp\left[\frac{-e_c|V_{sc}|}{\kappa T_e}\right] - J_{0i}A_n \left(1 + \frac{e_c|V_{sc}|}{\kappa T_i}\right)$$

$$(I_e - I_i)|_{V_{sc} > 0} = J_{0e}A_n \left(1 + \frac{e_c V_{sc}}{\kappa T_e}\right) - J_{0i}A_n \exp\left[\frac{-e_c V_{sc}}{\kappa T_i}\right]$$

⁹ Lai, Shu T. *Fundamentals of Spacecraft Charging: Spacecraft Interactions with Space Plasmas*. Princeton: Princeton University Press, 2012.

where $A_n \equiv 4\pi R_n^2$ is the surface area of the spherical node, $e_c \approx 1.6022 \times 10^{-19}$ C is the elementary charge, $\kappa \approx 1.3807 \times 10^{-23}$ J/K is the Boltzmann constant, T_e and T_i [K] are the local electron and proton temperatures, respectively, and J_{0e} and J_{0i} [A/m²] denote the saturation currents at $V_{sc} = 0$:¹⁰

$$J_{0e} = e_c n_e \sqrt{\frac{T'_e}{2\pi m_e}}$$

$$J_{0i} = e_c n_i \sqrt{\frac{T'_i}{2\pi m_i}}$$

where n_e and n_i are the single-Maxwellian electron and proton particle densities [cm⁻³] (assumed to be equivalent in this study), $T'_{e,i} = T_{e,i}/\kappa$ are local electron and proton particle energies [J] (also assumed equivalent), and m_e and m_i represent the electron and proton particle masses [kg]. The photoelectric current is an important contributor to current flow for a sunlit EIMS node, and is modeled as:

$$(-I_{Pe})|_{V_{sc} < 0} = -J_{0Pe} \left(\frac{A_n}{2}\right)$$

$$(-I_{Pe})|_{V_{sc} > 0} = -J_{0Pe} \left(\frac{A_n}{2}\right) \exp\left[\frac{-e_c V_{sc}}{\kappa T_{Pe}}\right] \left(1 + \frac{e_c V_{sc}}{\kappa T_{Pe}}\right)$$

where $J_{0Pe} = 20 \mu\text{A/m}^2$ is the saturation current density and T_{Pe} is the photoelectron temperature [K] (derived from mean photoelectron energy $T'_{e,i} = 2$ eV), chosen to represent typical spacecraft materials and provide a conservative estimate of the effect of photoelectric currents on EIMS power requirements. The term $A_n/2$ emphasizes that this current is computed with the sunlit hemisphere of the node only (ambient electron and proton currents are computed with the entire surface area). The power required to maintain a fixed EIMS potential is therefore computed with the expression:

$$P_{req} = |I_{cc} V_{sc}|$$

To assess the influence of a representative range of electron and proton densities and energies on the EIMS power requirement, two numerical parameter sweeps are performed: (a) particle densities $n_{e,i}$ varied from 0–50 cm⁻³ at nominal particle energy $T'_{e,i} = 40$ eV; (b) particle energies $T'_{e,i}$ varied from 0–50 eV at nominal particle density $n_{e,i} = 10$ cm⁻³. Note that the nominal conditions denote a Debye length $\lambda_D \approx 15$ m, representative of the deep space solar wind conditions at 1 AU. In each parameter sweep, the isolated EIMS potential V_{sc} is varied logarithmically from -100 MV to +100 MV.

The power requirements associated with the particle density sweep are illustrated in Figure 7.1; the power requirements corresponding to the particle energy sweep are depicted within Figure 7.2. To illustrate the power for a large range of conditions, the potential axis (horizontal axis) is shown on a logarithmic scale. A positive value x indicates a positive potential 10^x , while a negative value -3 indicates a negative potential of -10^3 , or -1kV. A mega-volt of potential would be thus at a value of 6 (i.e. 10^6 V). For

¹⁰ Hastings, Daniel, and Henry Garrett. *Spacecraft-Environment Interactions*. Cambridge: Cambridge University Press, 1996.

convenience, the nominal density and energy conditions are notated with dashed lines upon these power diagrams.

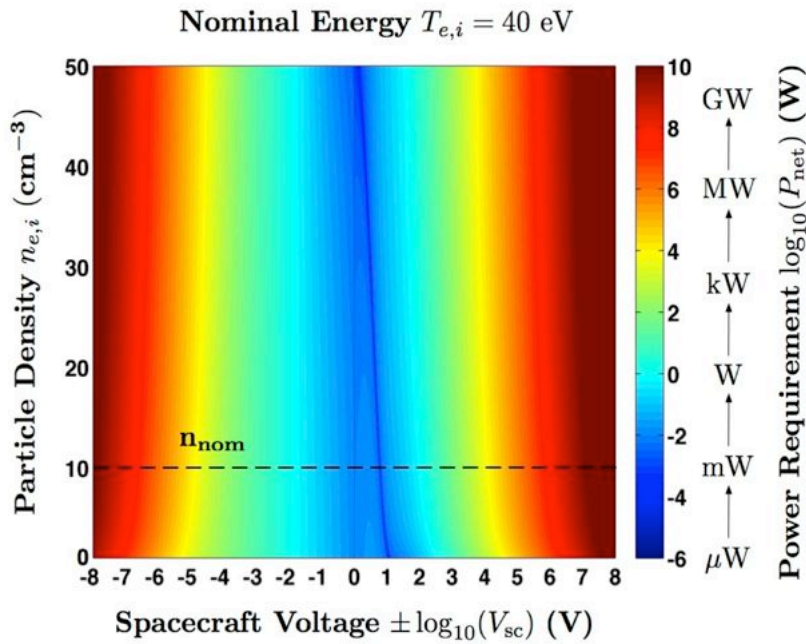


Figure 7.1: Power requirement for representative range of particle densities

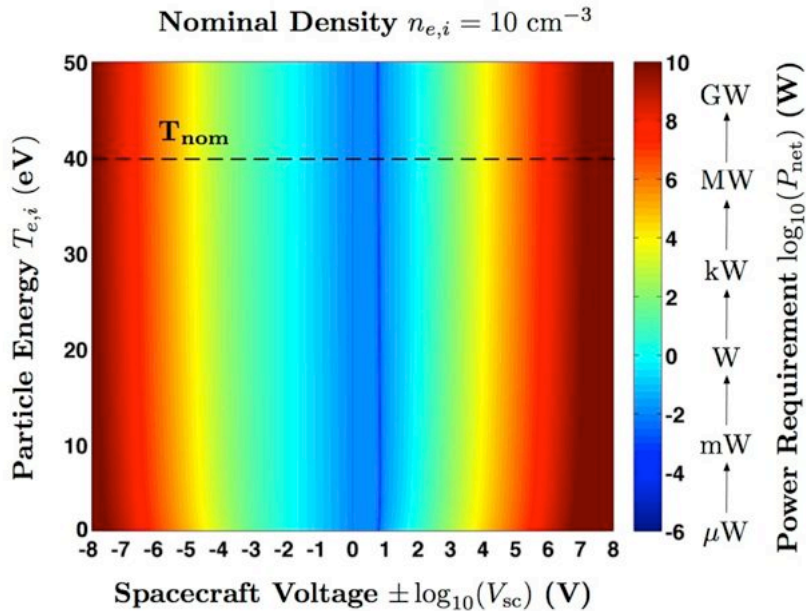


Figure 7.2: Power requirement for representative range of particle

Figure 7.1 and Figure 7.2 indicate that the EIMS power requirement becomes increasingly more challenging as the spacecraft voltage is increased, reaching kW to MW levels and higher for larger voltages. However, floating potentials in which the

natural equilibrium $I_{net} = 0$ is achieved are visible upon the power plots – these regions may be exploited to reduce slightly incurred EIMS power requirements. Though nominally in the negative potential regime, these useful floating potentials are positive in the presence of the photoelectron current. Charging to positive potentials yielded slightly smaller power needs.

7.2 SPE Power Requirement

For the power requirements investigated in this study, it is of interest to assess the effects of double-Maxwellian plasma distributions developed simultaneous interaction with the ambient plasma environment and that of a solar particle event (SPE). A representative SPE occurred in February 1956 and is summarized in Webber¹¹, from which the 1956 Webber differential [particles/cm²/MeV] and integral [particles/cm²] SPE spectrum is derived:

$$\frac{d\phi}{dE} = 10^7 \left(\frac{E + 938}{\sqrt{E(E + 1876)}} \right) \exp\{[239.1 - \sqrt{E(E + 1876)}]/100\}$$

$$\phi = 10^9 \exp\{[239.1 - \sqrt{E(E + 1876)}]/100\}$$

where E denotes particle energy in MeV. This Webber spectrum is exclusively a proton spectrum and is shown in Figure 7.3. Proton densities are required to evaluate the total current, and corresponding power requirements, of an isolated sphere within a double-Maxwellian plasma. Using the integral spectrum fluence data provided in Figure 7.3, the associated proton density spectrum is determined with:

$$n_p(E) = \frac{\phi}{\tau v}$$

where ϕ is the particle fluence, τ is the reference integration time, and $v = \sqrt{2E/m_p}$ is the velocity. For the February 1956 SPE, the reference time τ is given as 36 hours for particles with $E > 30$ MeV, and as 19 hours for particles with $E > 100$ MeV (reference time is computed as the sum of the SPE onset/rise and decay times provided in Reference 11). The proton density spectrum is computed and depicted in Figure 7.4. Only the portion of the integral Webber spectrum in Figure 7.3 satisfying $E > 30$ MeV is illustrated in Figure 7.4; reference times for less-energetic particles are not provided. Figure 7.4 indicates that for the range of representative SPE energies considered, the higher-energy constituents of the 1956 Webber proton spectrum will not have a strong influence upon the power requirements evaluated for this study. The densities associated with the high-energy particles is orders of magnitude lower than the low-energy particles. While these high-energy particles can be harmful to humans, they have a negligible impact on the electrostatic power requirement. Rather, the low-energy nominal space plasma conditions will dominate the power evaluations.

¹¹ Webber, W.R., "An Evaluation of the Radiation Hazard Due to Solar Particle Events," Boeing Report D2-90469, AeroSpace Division, The Boeing Company, 1963.

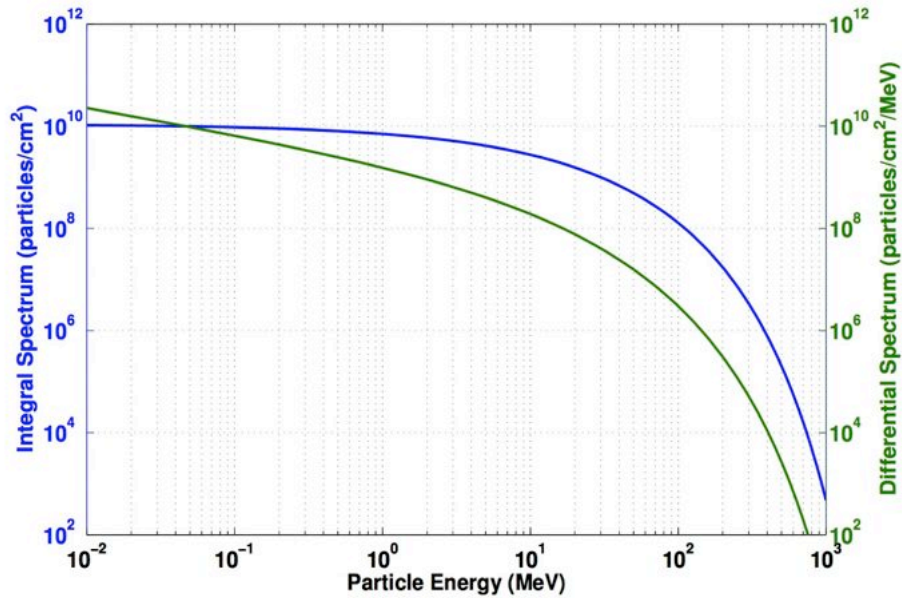


Figure 7.3: The February 1956 integral and differential SPE spectrum

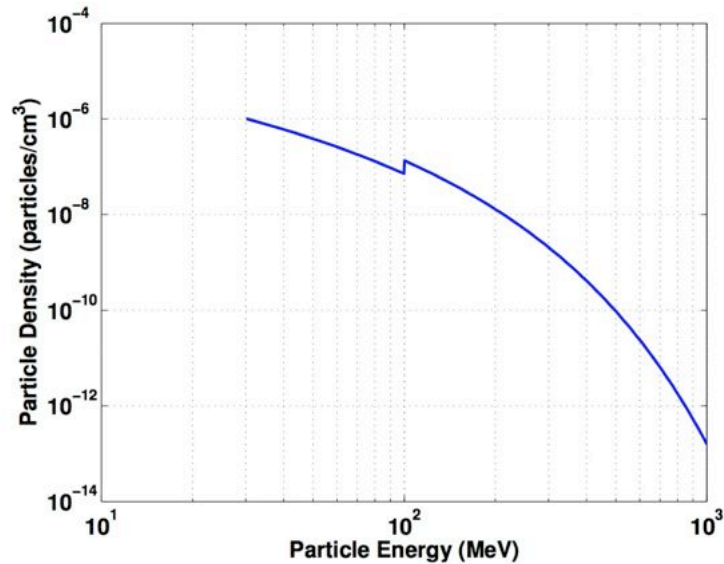


Figure 7.4: Proton density spectrum $n_p(E)$ for 1956 Webber

Employing a Langmuir attraction and Boltzmann repulsion model equivalent to that used to evaluate the nominal power magnitude, the power requirement for maintaining a fixed potential during a nominal SPE is therefore assessed. Figure 7.5 depicts this power requirement for a representative range of potential levels and proton energies. As illustrated, low SPE densities incur a power cost in the sub-Watt regime (nominally beneath the mW level for the majority of the parameter space). SPE thus do not affect the nominal power level required for an electrostatic radiation shielding system.

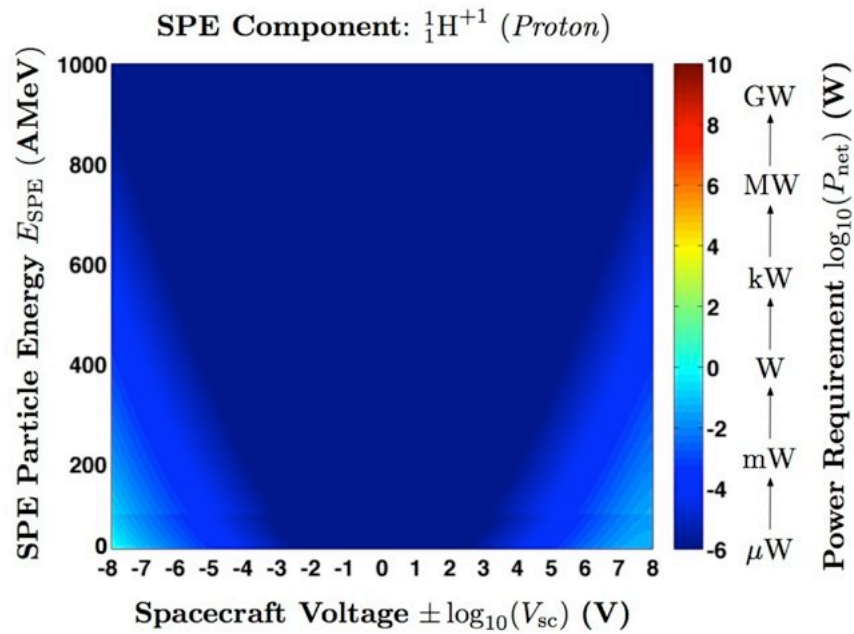


Figure 7.5: Contribution of nominal solar particle event to power requirement

7.3 GCR Power Requirement

To evaluate the effect of high-energy galactic cosmic radiation (GCR) on the nominal power requirement, a data file provided by NASA/Langley Research Center was similarly analyzed. Particle fluences for a variety of ions were converted into densities required for assessing the GCR power impact. As protons and alpha particles (helium nuclei) dominated this fluence data, only these two constituents were included in this power study. Therefore, implementing the Langmuir attraction and Boltzmann repulsion model, the GCR power requirement for a range of potential levels and particle energies was computed, and is shown in Figure 7.6.

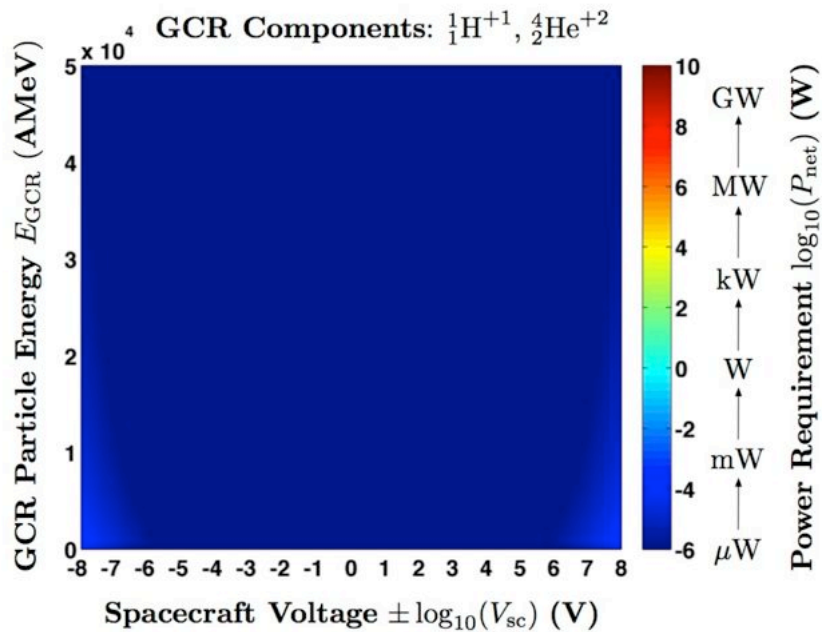


Figure 7.6: Contribution of nominal galactic cosmic radiation to power level

As indicated, the low densities associated with the representative range of particle energies incur a power cost beneath the mW level. As this order of power magnitude is effectively negligible, GCR do not affect the nominal power level required for an electrostatic shielding system. Though the high energies associated with GCR are damaging to human tissue and are thus threatening from a human factors viewpoint, the low densities associated with such energies ensure that the power requirement is insignificant.

7.4 Outlook

The challenges of designing a robust, yet power-efficient node configuration for active radiation shielding are illustrated in Figure 7.7 for a nominal deep-space solar wind energy of 40 eV. These negatively-charged *red* nodes are of 20-m radius and are held at -17 kV; the positively-charged *green* nodes are of 10-m radius and are held at 35 kV. As observed in Figure 7.7, though the positive nodes are charged to a higher potential, they don't experience any current arising from the plasma influx – therefore, in this situation, the power requirement is driven by the ion currents experienced by the negative nodes on the outside of the deflection configuration, which require active charge control to maintain the desired potential level. The challenge for designing an efficient deflection scheme that is robust to variable space weather conditions lies in the ability to balance node size, position, and potential in an optimal, effective, and power-efficient manner.

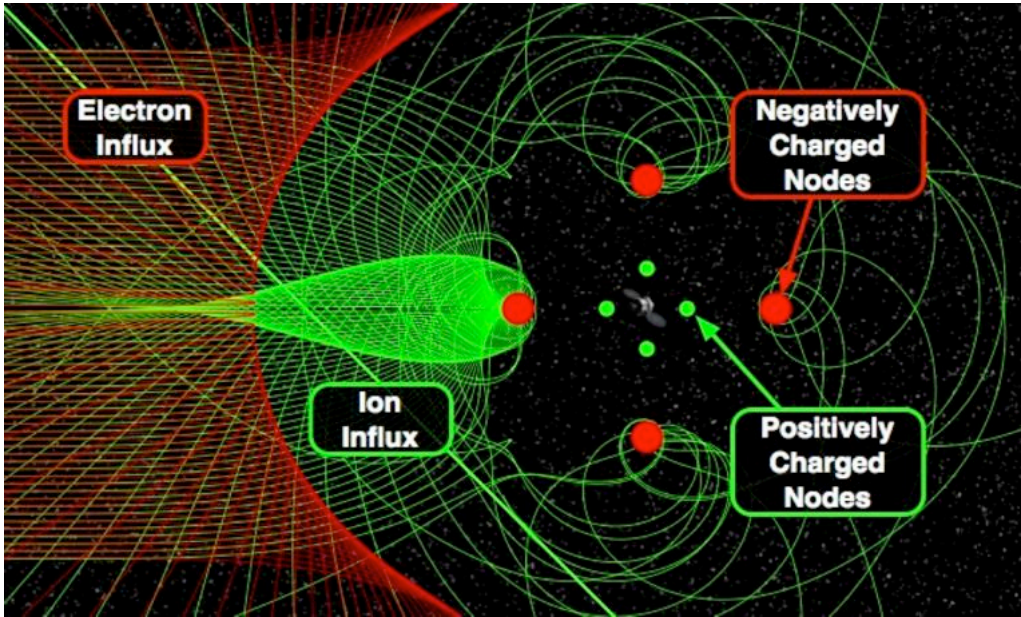


Figure 7.7: Electrostatic deflection for active space radiation shielding with charged nodes

8 Conclusions

This report summarizes research performed on the use of electrostatically inflated membrane structures for active radiation shielding. The study focused on the small membrane vibrations observed during charge bombardment of an EIMS. Elimination of several potential vibration sources led to the hypothesis that the vibration is a result of local surface charge density variations caused by the charge flux. Within this project, charge deflection and shielding experiments were performed. Plots were presented to describe both the shielding capabilities and the charge deflection patterns around a charged membrane, showing the capability to shield low-energy electrons with EIMS. Also, different membrane materials were investigated, including membrane of much smaller thickness. Thinner materials presented challenges in vacuum preparation and that rapid charging can melt the membrane. Results from the power requirements study show that the EIMS power requirement becomes increasingly more challenging as the spacecraft voltage is increased, reaching kW to MW levels for larger voltages. It was found, though, that SPE and GCR do not affect the nominal power level required for an electrostatic radiation shielding system.